Electrochimica Acta 146 (2014) 585–590

Contents lists available at ScienceDirect

Electrochimica Acta

journal homepage: www.elsevier.com/locate/electacta

Octagonal prism shaped lithium iron phosphate composite particles as positive electrode materials for rechargeable lithium-ion battery

Keqiang Ding[a,*], Hongbo Gu[a,b], Chunbao Zheng[a], Lu Liu[a], Likun Liu[a], Xingru Yan[b], Zhanhu Guo[b,**]

[a] College of Chemistry and Materials Science, Hebei Normal University, Shijiazhuang 050024, P.R. China
[b] Integrated Composites Laboratory (ICL), Dan F. Smith Department of Chemical Engineering, Lamar University, Beaumont, TX 77710, USA

ARTICLE INFO

Article history:
Received 1 July 2014
Received in revised form 21 August 2014
Accepted 26 August 2014
Available online 21 September 2014

Keywords:
Octagonal prism shape
lithium iron phosphate composites
multi-walled carbon nanotubes
Lithium ion battery

ABSTRACT

For the first time, octagonal prism shaped lithium iron phosphate ($LiFePO_4$) composite particles supported on the multi-walled carbon nanotubes (MWNTs) (denoted as OP-$LiFePO_4$/MWNTs) are prepared by using a boiling reflux assisted calcination method. Interestingly, spherical $LiFePO_4$ composite particles (indexed as S-$LiFePO_4$/C) are produced by the same procedure in the presence of activated carbon. It is observed that the edge length of OP-$LiFePO_4$ particles is about 400 nm as compared to the particle size of S-$LiFePO_4$ (~150 nm) sample. Cyclic voltammetry (CV) tests demonstrate that at the scan rate of 0.5 mVs^{-1} the potential separation of the OP-$LiFePO_4$ sample (about 250 mV) is much smaller than that of S-$LiFePO_4$ (about 443 mV). More importantly, the initial discharge capacities at 0.1 and 1.0 C for the OP-$LiFePO_4$/MWNTs are 160.58 and 116.71 $mAhg^{-1}$, higher than that of S-$LiFePO_4$/C (151.29 and 95.69 $mAhg^{-1}$ at 0.1 and 1.0 C).

1. Introduction

Lithium ion batteries (LIBs) are one of the most advanced secondary rechargeable energy storage devices due to its higher power and energy density [1–3]. The development of higher energy LIBs is essential for the further commercialization of portable electronic devices [4], such as laptops, personal digital assistants, cellular phones, and automotives [5]. Recently, olivine structured lithium iron phosphate ($LiFePO_4$) has been thought as a promising cathode candidate for the higher power LIBs especially since its discovery by Goodenough group [6]. $LiFePO_4$ has a theoretical specific capacity of 170 mAh g^{-1} and a relatively high redox potential of 3.4 ~ 3.5 V *vs.* Li/Li^+ arising from the chemical valence transition of the Fe^{2+}/Fe^{3+} couple [7,8]. However, the disadvantages of $LiFePO_4$ including the lower electronic conductivity (10^{-9} S cm^{-1}) and lower lithium ion diffusion coefficient (10^{-18} m^2 s^{-1}) effectively limit its wide applications [9,10]. Thus, many methods have been developed to resolve above problems. Summarily, the following three solutions were proposed so far, (i) anchoring a conductive layer on the surface of the particles; (ii) doping a second (or third) metal ion into the lattice of crystallite $LiFePO_4$; (iii) controlling the morphologies of the resultant $LiFePO_4$ particles.

Up to now, many works concerning the morphologies of the $LiFePO_4$ particles have been published. For example, Xing et al. [11] reported the synthesis of $LiFePO_4$ particles that have a 3D conductive network and porous structure, and he addressed that the as-prepared sample could deliver a discharge capacity of 95 mAh g^{-1} at a rate of 20 C. Sun et al. [12] synthesized $LiFePO_4$ microspheres that consist of nanoplates or nanoparticles by using a novel solvothermal method, and after mixing with carbon materials the products exhibited larger discharge capacity values (140 mAh g^{-1} at 0.1 C) and better cycling performance (110 mAh g^{-1} at 5 C and 86 mAh g^{-1} at 10 C after 1000 cycles). Chen et al. [13] fabricated the monodisperse porous $LiFePO_4$/C microspheres with a diameter range of 1.0 ~ 1.5 μm *via* a microwave-assisted hydrothermal approach combined with carbothermal reduction. Wang et al. [14] fabricated nano-sized core-shell structured $LiFePO_4$/C nanocomposites using polyaniline (PANI) as the carbon precursor. Lim et al. [15] synthesized the nanowire and hollow particles of $LiFePO_4$, in which the nanowire sample showed a discharge capacity of 157 mAh g^{-1} at 0.2 C and the hollow sample exhibited a discharge capacity of 165 mAh g^{-1} at 0.2 C. Muraliganth et al. [16] reported that the $LiFePO_4$ nanorods could be prepared by a rapid microwave-solvothermal method within 5 minutes at the temperature of 300 °C. Zhou et al. [17]

* Corresponding author. Tel.: +86-311-80787400; fax: +86-311-80787401.
** Corresponding author. Tel.: +(409) 880-7654/7195; fax: +(409) 880-2197.
E-mail addresses: dkeqiang@263.net (K. Ding), zhanhu.guo@lamar.edu (Z. Guo).

http://dx.doi.org/10.1016/j.electacta.2014.08.141
0013-4686/

described the synthesis of a highly-conductive 3D carbon nanotube network interlaced with porous $LiFePO_4$ through an in-situ sol-gel process, which exhibited a discharge capacity of 159 mAh g^{-1} at the current density of 10 mA g^{-1}. Toprakci et al. [18] prepared the $LiFePO_4$/CNT/C composite nanofibers through a combined method (electrospinning and sol-gel techniques), and the as-prepared samples displayed large capacity value (165 mAh g^{-1} at 0.1 C), extended cycle life, and excellent rate capability. It can be deduced from above publications that the carbon sources played a key role in controlling the morphology of the resultant $LiFePO_4$ particles. To the best of our knowledge, there is no paper reporting the preparation of octagonal prism shaped $LiFePO_4$ huge particles and the method of boiling reflux assisted calcination process as well.

In this communication, MWNTs and activated carbon have been utilized as carbon sources in the boiling reflux assisted calcination process for preparing $LiFePO_4$, with an intention to evaluate the influence of carbon sources on the morphologies of the resultant samples. As a result, octagonal prism shaped and spherical particles of $LiFePO_4$ were produced, respectively, in the presence of MWNTs and activated carbon. The obtained $LiFePO_4$ composites have been characterized by Fourier transform infrared (FT-IR), X-ray diffraction (XRD), Energy Dispersive X-Ray Spectroscopy (EDX), and scanning electron microscope (SEM). The electrochemical performances of the $LiFePO_4$ composites as cathode materials for the LIBs are evaluated by cyclic voltammetry (CV), electrochemical impedance spectroscopy (EIS), and galvanostatic charge-discharge measurement.

2. Experimental

$LiOH{\cdot}H_2O$ (99.0 wt%), phosphoric acid (H_3PO_4, 85 wt%), α-Fe_2O_3, activated carbon, oxalic acid ($\geq$ 99.5 wt%), and glucose were all obtained from Tianjin Yongda Chemical Reagent Co., Ltd (China). Acetylene black, polyvinylidene fluoride (PVDF, binder), N-methyl-2-pyrrolidone (NMP), electrolyte solution (ethylene carbonate (EC)/diethyl carbonate (DEC)/dimethyl carbonate (DMC) = 2: 5: 11 (volume) with 1 mol L^{-1} $LiClO_4$), and polypropylene (PP, M_w = 2400) were purchased from Tianjin Liangnuo S&T Development Co., Ltd (China). Multi-walled carbon nanotubes (MWNTs) with an average diameter of 30 $\sim$ 50 nm were purchased from Shenzhen Nanotech Port Co., Ltd. (China). All of the chemicals were analytical grade and used as-received without any further treatment. Doubly distilled water was used to prepare the aqueous solutions.

The procedure for the preparation of $LiFePO_4$ composites filled with MWNTs or activated carbon is as follows. Starting materials of $LiOH{\cdot}H_2O$, H_3PO_4, α-Fe_2O_3 and MWNTs in a molar ratio of 1.1: 1: 0.5: 0.6 were mixed with 90 mL distilled water in a three-neck round-bottom flask. 5 g of oxalic acid and 0.4 g glucose were added into the above suspension solution, and then the suspension solution was heated to boiling reflux, and this process was kept for about one hour until the solution volume became 30 $\sim$ 40 mL. It should be noted that after the boiling reflux process, a green solution was obtained, indicative of the Fe^{2+} formation. After cooling down to the room temperature, the solution was placed in an oven and dried at 150 °C for 3 h. Subsequently, the produced powders were ground in a mortar and pressed into a slice with a diameter of around 1 cm. And then the samples were transferred into a crucible that was covered by carbon powders. Finally, the crucible was placed in an electronic furnace at 700 °C for 5 h. The final product was denoted as OP-$LiFePO_4$/MWNTs. The products mixed with activated carbon were also fabricated according to the same procedure, and correspondingly, the resultant samples were named as S-$LiFePO_4$/C.

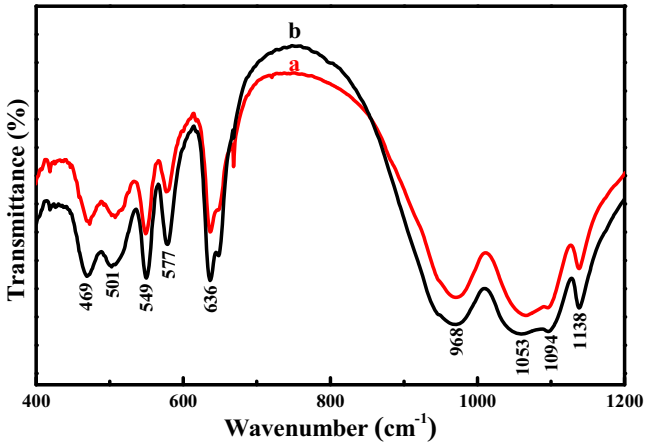

Fig. 1. FT-IR spectra of (a) OP-$LiFePO_4$/MWNTs and (b) S-$LiFePO_4$/C samples.

Fourier transform infrared (FT-IR) spectra of the samples were obtained on a JASCO 8900 (Hitachi Ltd., Japan) in the range of 400 to 1200 cm^{-1} at a resolution of 4 cm^{-1}. X-ray diffraction (XRD) analysis was carried out with a Bruker AXS D8 ADVANCES with a Cu-Kα radiation source (λ = 1.5406 Å). Data were collected in a range of 15 to 75°. The morphologies of the synthesized products were observed on a field emission scanning electron microscope (SEM, S-4800, Hitachi Ltd., Japan). Energy Dispersive X-ray Spectroscopy (EDX) spectrum analysis was carried out on an instrument of EDAX (PV-9900, USA).

Electrochemical measurements were carried out on a CHI 660B electrochemical workstation (Shanghai Chenhua Apparatus, China) connected to a personal computer. In the EIS measurement, the excitation voltage applied to the cells was 5 mV and the frequency range was from 0.1 to 1 $\times$ 10^5 Hz. All the experiments were carried out at room temperature.

The cathode was prepared as follows. The fabricated OP-$LiFePO_4$/MWNTs or S-$LiFePO_4$/C powders, polyvinylidene fluoride (PVDF), acetylene black were mixed in n-methyl-2 pyrrolidone (NMP) solution with a weight ratio of 8: 1: 1. After the above slurries were uniformly coated on the aluminum foil with a diameter of 10 mm, the prepared electrodes were put into a vacuum oven and dried at 120 °C for 12 h. After that, the dried samples were pressed by hydraulic presser at 5 MPa and cut into disks before transferring into a nitrogen-filled glove box. Two-electrode electrochemical cells, consisting of lithium metal foil as the negative electrode, Celgard 2400 separator, and an electrolyte of 1 M $LiClO_4$ in ethylene carbonate (EC):diethyl carbonate(DEC):dimethyl carbonate (DMC) (2:5:11, vol.), were assembled in a nitrogen-filled glove box. The electrochemical cycle tests were performed using a CT-3008W-5V20mA-S4 testing system (Shen Zhen Newware Technology Ltd., China) at various rates (1 C = 170 mAh g^{-1}) between 2.75 and 4.2 V at room temperature.

3. Results and discussion

Fig. 1 shows the FT-IR spectra of OP-$LiFePO_4$/MWNTs and S-$LiFePO_4$/C samples. The main absorption bands are in the region of 400 $\sim$ 1200 cm^{-1}. The strong bands at 636, 968, 1053, 1094, and 1138 cm^{-1} correspond to the symmetrical and asymmetrical vibration of PO_4^{3-} [19]. The peaks located at 469, 501, 549, and 577 cm^{-1} are assigned to the bending vibration of P-O band. These characteristic peaks (469, 501, 549, 577 636, 968, 1053, 1094, and 1138 cm^{-1}) are consistent with the results of $LiFePO_4$ in the literature [19] very well. Fig. 2 shows the EDX spectra of $LiFePO_4$/MWNTs and $LiFePO_4$/C samples. Only Fe, P, O elements are observed in the OP-$LiFePO_4$/MWNTs and S-$LiFePO_4$/C samples, indicating that there

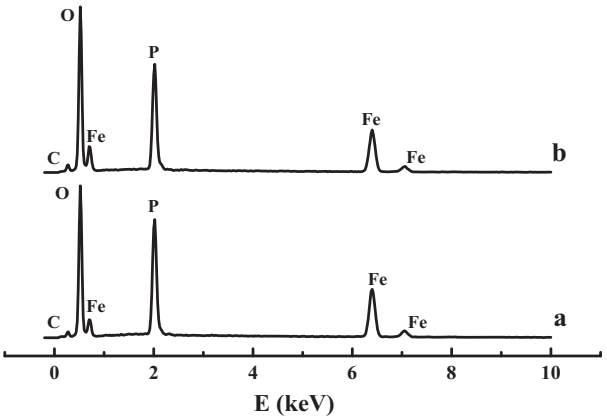

Fig. 2. EDX spectra of (a) OP-$LiFePO_4$/MWNTs and (b) S-$LiFePO_4$/C samples.

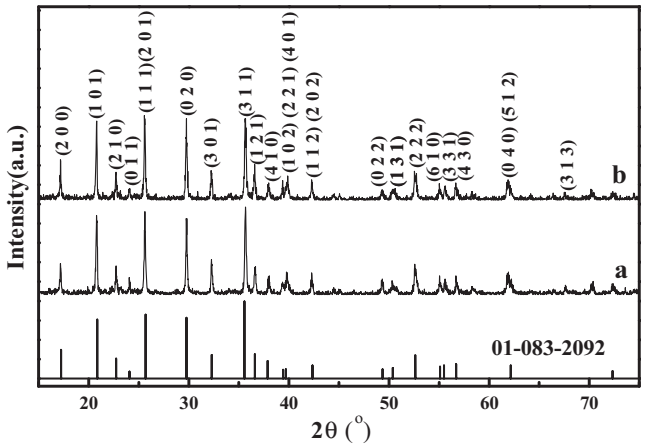

Fig. 3. XRD patterns of (a) OP-$LiFePO_4$/MWNTs and (b) S-$LiFePO_4$/C samples.

are no other impurities such as SO_4^{2-} and NO_3^- introduced during the formation of $LiFePO_4$ [20]. Li element cannot be detected by this technique due to the low atomic weight of Li [21]. The weight percentages of Fe, P, O elements in the OP-$LiFePO_4$/MWNTs sample are observed to be 22.10, 16.87 and 56.21%, respectively. The weight percentages of Fe, P, O elements in the S-$LiFePO_4$/C sample are 19.30, 14.00, and 59.24%, respectively. This result indicated that the components of the OP-$LiFePO_4$/MWNTs and S-$LiFePO_4$/C are close to each other.

The X-ray diffraction (XRD) patterns of OP-$LiFePO_4$/MWNTs and S-$LiFePO_4$/C samples are shown in Fig. 3. The XRD patterns of OP-$LiFePO_4$/MWNTs and S-$LiFePO_4$/C samples are consistent with the standard pattern of $LiFePO_4$ (JCPDS#01-083-2092) very well, indicating a single phase of olivine $LiFePO_4$ structure with the orthorhombic crystal structure[22]. Meanwhile, no other diffraction peaks are observed in the XRD patterns of above two samples. These indicated that both the OP-$LiFePO_4$/MWNTs and S-$LiFePO_4$/C samples have only the olivine crystal structure. In addition, no diffraction peak of carbon structure (normally located at $2\theta = 25^\circ$ corresponding to the (0 0 2) facet of the carbon materials [23]) is observed probably due to its disordered state and/or low content in the composites. This indicated that the addition of MWNTs and activated carbon has no effect on the crystal structure of olivine $LiFePO_4$.

Fig. 4 shows the SEM images of OP-$LiFePO_4$/MWNTs and S-$LiFePO_4$/C samples. Interestingly, the $LiFeO_4$ composites exhibited different morphologies when using different carbon sources. It is clear that for the OP-$LiFePO_4$/MWNTs sample, octagonal prism shaped huge particles (circled part) were found in the MWNTs, Fig. 4(a & c). Close inspection revealed that the length of the huge particle was about 400 nm and the diameter of its section was around 130 nm. The shape of OP-$LiFePO_4$ particles presented here is novel, as has never been reported previously. Interestingly, the S-$LiFeO_4$ particles prepared in the presence of activated carbon showed a ball-like structure with an average diameter around 150 nm, Fig. 4(b & d).

The electrochemical performance of the as-prepared battery cell was characterized by the cyclic voltammetry (CV), galvanostatic charge/discharge, and EIS measurements. Fig. 5 shows the CVs of

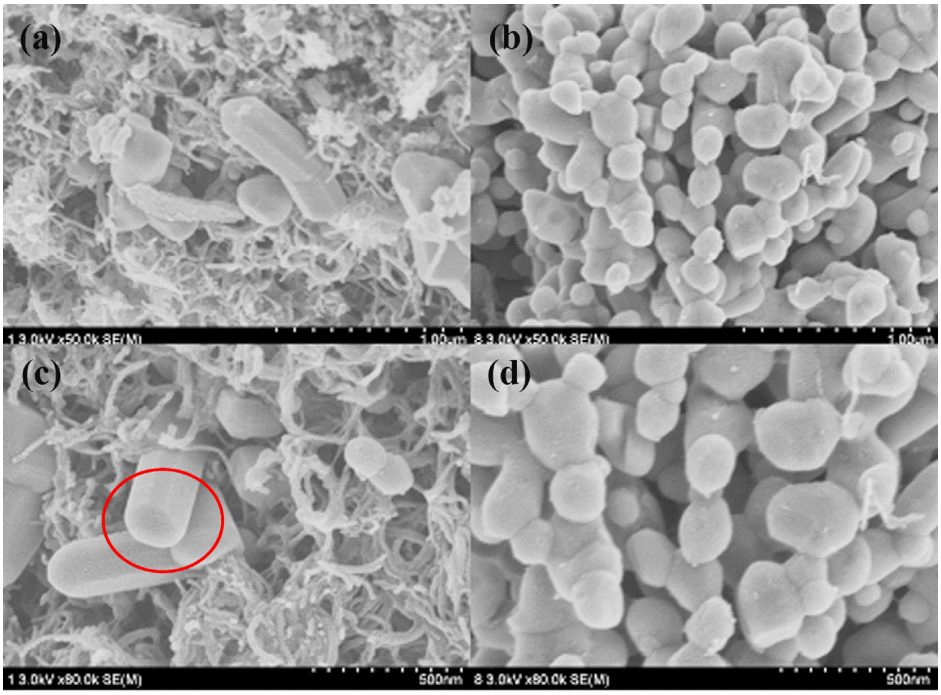

Fig. 4. SEM images of (a) OP-$LiFePO_4$/MWNTs, and (b) S-$LiFePO_4$/C samples; Enlarged SEM images of (c) OP-$LiFePO_4$/MWNTs, and (d) S-$LiFePO_4$/C samples.

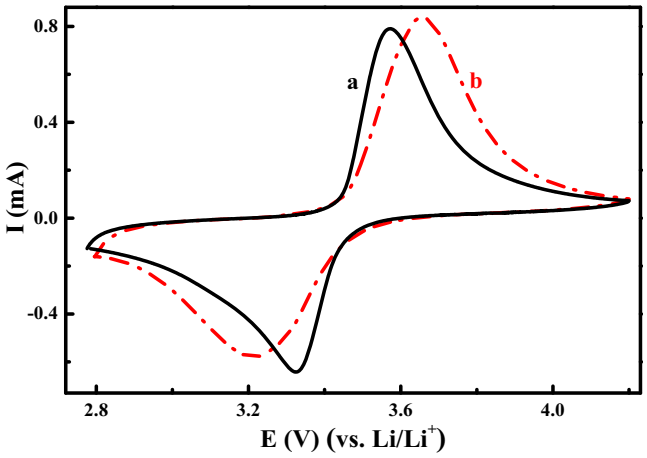

Fig. 5. CV curves of (a) OP-$LiFePO_4$/MWNTs and (b) S-$LiFePO_4$/C samples.

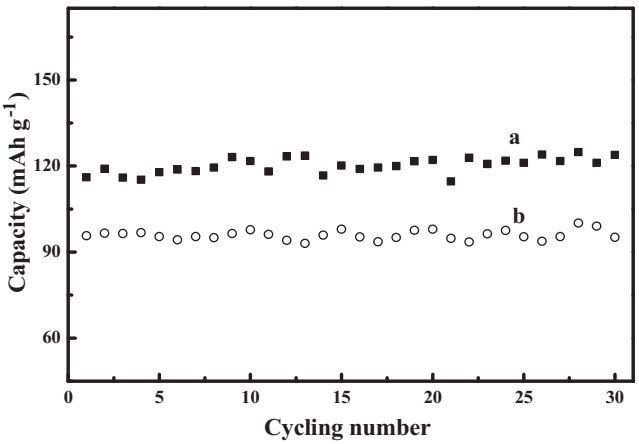

Fig. 7. Cycling performance of the discharge capacity for the cell (a) OP-$LiFePO_4$/MWNTs and (b) S-$LiFePO_4$/C samples at rate of 1C.

the battery cell assembled by the as-prepared OP-$LiFePO_4$/MWNTs and S-$LiFePO_4$/C samples at a potential scanning rate of 0.5 mV s^{-1}. Both samples exhibited one pair of well-defined redox peak, which corresponds to the extraction and insertion of Li ion during the electrochemical reaction [24]. The oxidation and reduction peak potentials for OP-$LiFePO_4$/MWNTs sample are 3.573 and 3.323 V, respectively. For the S-$LiFePO_4$/C sample, the oxidation and reduction peak potentials are 3.655 and 3.212 V, respectively. The peak potential intervals between oxidation and reduction peaks (ΔE_p, $\Delta E_p = E_{pa} - E_{pc}$, where E_{pa} and E_{pc} are the peak potentials for anodic and cathodic reaction, respectively) for OP-$LiFePO_4$/MWNTs and S-$LiFePO_4$/C samples are approximately 250 and 443 mV, respectively. Generally, the more broadened the peak interval, the higher the electrode polarization. And a smaller peak potential separation indicates a better reversibility of a battery cell [25]. Therefore, the reversibility for the intercalation/deintercalation process of the Li ions in the OP-$LiFePO_4$/MWNTs is much better than that in the S-$LiFePO_4$/C, even though the peak current of the OP-$LiFePO_4$/MWNTs is slightly lower than that of S-$LiFePO_4$/C sample.

Fig. 6 shows the initial charge-discharge curves of the prepared cells at the rates of 0.1 and 1 C with a potential window ranging from 2.75 to 4.2 V. The capacity values of the OP-$LiFePO_4$/MWNTs and S-$LiFePO_4$/C samples in the initial discharge cycle at the rate of 0.1 C are 160.58 and 151.29 mAh g^{-1}, respectively, which is much better than the results obtained by Ziolkowska et al. (122 mAh g^{-1} for the Sn-modified $LiFePO_4$ material) [26]. In the charge/discharge profile, only one voltage plateau is observed, which corresponds

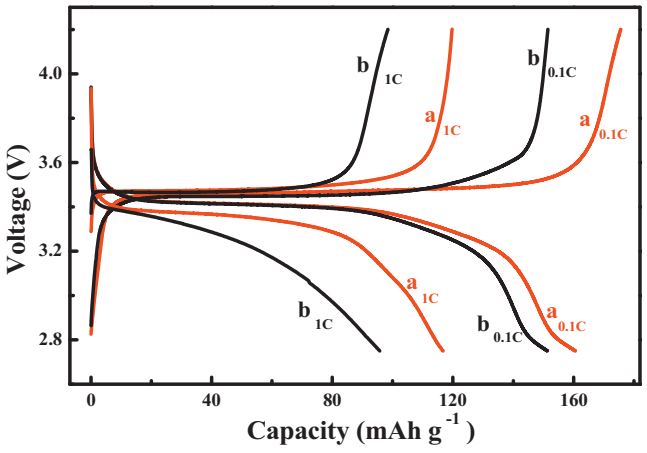

Fig. 6. Charge and discharge curves of the battery cell (a) OP-$LiFePO_4$/MWNTs and (b) S-$LiFePO_4$/C samples at different rates.

to the extraction/insertion process of Li ions and two phase transformation reactions between $LiFePO_4$ and $FePO_4$ [27]. This result is consistent with that obtained from the CV curve, Fig. 5. The voltage interval bettween the charge and discharge voltage plateaus is normally related to the polarization loss [28] and the reversibility of a battery cell [29]. In Fig. 6, the voltage intervals between the charge and discharge voltage plateaus for OP-$LiFePO_4$/MWNTs and S-$LiFePO_4$/C samples are 50.9 and 52.9 mV, respectively. Therefore, the reversiblility of the cell assembled by OP-$LiFePO_4$/MWNTs sample was better than that in S-$LiFePO_4$/C sample [30].

After increasing the rate to 1 C, the discharge capacity values of OP-$LiFePO_4$/MWNTs and S-$LiFePO_4$/C samples for the initial discharge cycle dropped to 116.7 and 95.69 mAh g^{-1}, respectively. Thus, it can be concluded that the discharge capacity of OP-$LiFePO_4$/MWNTs sample is much higher than that of S-$LiFePO_4$/C sample. The discharge potential plateau of OP-$LiFePO_4$/MWNTs sample is located at about 3.36 V, and no obvious flat discharge potential plateau is observed in the case of S-$LiFePO_4$/C sample. Thus, the electrochemical properties of OP-$LiFePO_4$/MWNTs sample are superior to those of S-$LiFePO_4$/C sample in terms of the discharge capacity value, discharge voltage plateau and reversibility even at a higher rate of 1C.

The cycling performance of the prepared cells made from OP-$LiFePO_4$/MWNTs and S-$LiFePO_4$/C samples is also investigated. Fig. 7 shows the discharge capacities of OP-$LiFePO_4$/MWNTs and S-$LiFePO_4$/C samples during the 30 charge-discharge cycles at a current rate of 1 C. The capacity values for both battery cells are well maintained even after 30 cycles. For example, in the whole testing period, the discharge capacity value of OP-$LiFePO_4$/MWNTs sample was at around 120 mAh g^{-1}, higher than that of S-$LiFePO_4$/C sample (around 100 mAh g^{-1}). This result substantially indicated that both samples have excellent cycling stability. Fig. 8 shows the rate capabilities of these two samples measured at 0.1C, 0.5C, 1C and 1.5C rates during every five cycles. It is evident that the discharge capacity value decreased with increasing C rate. This is mainly due to the increased IR voltage loss and higher concentration polarization at the electrode/electrolyte interface to meet the fast reaction kinetics at higher C rates [31]. Evidently, the discharge capacity values of OP-$LiFePO_4$/MWNTs and S-$LiFePO_4$/C at 0.1 C and 1.5 C are, 160 and 90 mAh g^{-1}, 150 and 76 mAh g^{-1}, respectively. That is to say, the discharge capacity value of OP-$LiFePO_4$/MWNTs sample is always higher than that of S-$LiFePO_4$/C when applied by the same current rates. Interestingly, when reset to a 0.1C discharging rate after 20 cycles, the discharge capacities for OP-$LiFePO_4$/MWNTs and S-$LiFePO_4$/C samples are still 160 and 152 mAh g^{-1}, respectively.

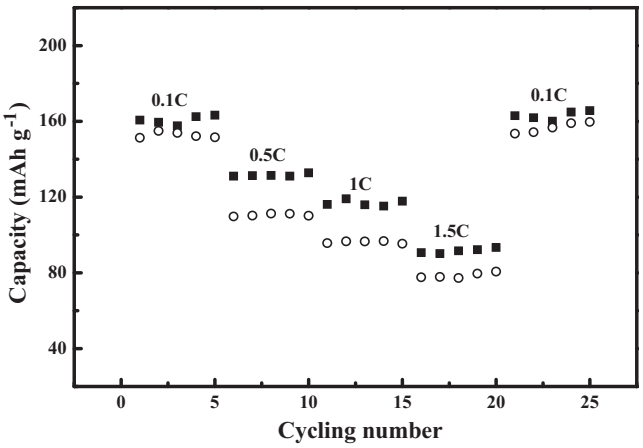

Fig. 8. Cycling performance of the discharge capacity for the battery cell (a) OP-$LiFePO_4$/MWNTs and (b) S-$LiFePO_4$/C samples at different rates.

These values are almost the same as the discharge capacities after 5 cycles (0.1C) before the high-rate discharge (0.5C, 1C and 1.5C), indicating a good capacity retention.

The EIS measurements were carried out in the frequency range from 0.1 to 10^5 Hz. The inset of Fig. 9 shows the typical Nyquist plots. Generally, in the Nyquist plots, the semi-circle at the high frequency region stands for the charge-transfer-limited process at the interface of electrodes and the inclined line at the low frequency region represents the Warburg factor being associated with the diffusion-limited process of the Li ions in $LiFePO_4$ [32]. And the numerical value of the diameter of the semicircle on the Z' axis is approximately equal to charge transfer resistance (R_{ct}). Thus, values of R_{ct} for the OP-$LiFePO_4$/MWNTs and S-$LiFePO_4$/C samples are estimated to be 50 and 81 Ω, respectively. This illustrates that the intercalation/deintercalation process of Li ion in the OP-$LiFePO_4$/MWNTs sample battery cell is much easier than that in the S-$LiFePO_4$/C sample assembled cell.

Normally, the diffusion coefficient (D) of Li ions in the solid phase of a battery cell can be calculated from Equation (1) [33]:

$$D = (R^2T^2)/(2A^2n^4F^4c^2\sigma^2) \quad (1)$$

where R is the gas constant (8.314 J mol K^{-1}), T is the absulute temperature (K); A is the effective surface area per unit of the athode; n is the transfer number of electrons *per* molecule during oxidization; F is the Faraday constant; c is the concentration of Li ions in the solid phase, which normally is 7.69×10^{-3} mol cm^{-3} [34]; σ is the Warburg prefactor, which can be determined from the slope of the $Z' \sim \omega^{-1/2}$ curve based on the following relationship [34], in which R_s is the resistance of SPE(solid polymer electrolyte), and R_{ct} is the charge transfer resistance.

$$Z' = R_s + R_{ct} + \sigma\omega^{-1/2} \quad (2)$$

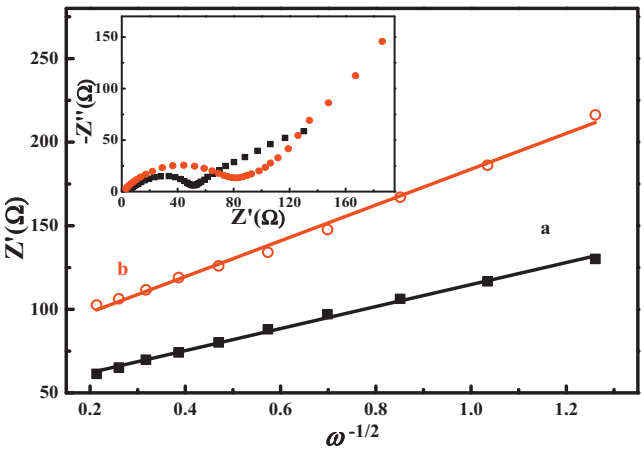

Fig. 9. Z' as a function of $\omega^{-1/2}$ of (a) OP-$LiFePO_4$/MWNTs and (b) S-$LiFePO_4$/C samples at low frequency range. Inset shows the Nyquist plots of (a) OP-$LiFePO_4$/MWNTs and (b) S-$LiFePO_4$/C samples.

Fig. 9 shows the relationship between Z' and the reciprocal square root of frequency ($\omega^{-1/2}$) in the low frequency region. The corresponding values D of Li ions in OP-$LiFePO_4$/MWNTs and S-$LiFePO_4$/C samples are calculated to be 1.45×10^{-14} and 5.53×10^{-15} cm^2 s^{-1}, respectively. This result indicates that the diffusion process of Li ions (which is the slowest process) into OP-$LiFePO_4$/MWNTs sample is easier than that in S-$LiFePO_4$/C sample. This result is consistent with the results obtained in Nyquist plots, in which the higher conductivity is observed in OP-$LiFePO_4$/MWNTs sample. The decreased charge transfer resistance and increased Li ion diffusion coefficient should be responsible for the higher discharge capacity (160.58 mAh g^{-1} at 0.1C) in the OP-$LiFePO_4$/MWNTs composite.

Generally, it is thought that smaller $LiFePO_4$ nanoparticles are beneficial for the diffusion of Li ions due to their ability of shortening the diffusion path of Li-ions [35]. However, in this work, the larger particles of OP-$LiFePO_4$ composites showed significantly enhanced electrochemical performance as compared to the smaller particles of S-$LiFePO_4$, which is rather opposite to the previous proposition that in $LiFePO_4$-based cathode materials the electrode resistance depends solely on the mean particle size. How does one under this interesting result? Up to now, several factors, such as, electrical conductivity, particle size and crystallinity of crystal particles, have been thought as the main factors that can greatly affect the electrochemical performance of a cathode material. In this work, a new concept, i.e., "order degree of arrangement" of particles, was tentatively proposed. That is to say, due to the well defined crystal structure and the huge particle size, the OP-$LiFePO_4$ particles, when being pressed to form an electrode, can be arranged much more orderly as compared to the case of S-$LiFePO_4$ particles. Additionally, it has been reported that Li-ions diffusion mainly proceeded along the shortest axis (c-axis) in a lattice [36]. Thus, the direction selectivity of Li-ions diffusion in the OP-$LiFePO_4$ huge particles structured cathode was superior to that in the cathode constituted by smaller particles of S-$LiFePO_4$. These novel concepts proposed here, i.e., "order degree of arrangement" and "direction selectivity of Li-ions diffusion", probably can be well utilized to interpret some facts that larger particles of $LiFePO_4$ as cathode materials could also exhibit excellent electrochemical performance as reported in Ref.[17] and [29].

How does one under the formation process of such huge particles OP-$LiFePO_4$ in this novel work? According to our previous work [37], during the boiling reflux process, all metal ions may spontaneously assembled on the surface of MWNTs due to the van der Waals forces or the so called chemical interaction between metal ions and the organic groups that existed on the surface of MWNTs, leading to the formation of a so-called self-assembled monolayer [38]. And during the annealing process, due to the well arranged assembly of metal ions and anions, orderly arrayed molecules are produced in the vicinity of MWNTs. As a result, crystal particles of $LiFePO_4$ would grow up along their preferential growth direction, leading to the generation of huge crystal particles of OP-$LiFePO_4$. In other words, in above process, MWNTs acted as an initiator for the ordered arrangement of metal ions, which may lead to the ordered assembly of prepared molecules. Or in other words, ordered arrangement of ions produced ordered assembly of molecules, and the well arranged molecules could produce well accumulated nanoparticles. Consequently, huge particles with a

special morphology were fabricated. Evidently, the morphology of the activated carbon was rather different from that of MWNTs, exhibiting various properties when being employed in this developed process. It is expected that the prepared OP-$LiFePO_4$ huge particles have potential applications in the field of micro- electronic devices.

4. Conclusions

The octagonal prism shaped $LiFePO_4$/MWNTs and spherical $LiFePO_4$/C composites have been prepared *via* a boiling reflux assisted annealing method. The FT-IR spectra, EDX spectra, XRD measurement, and SEM technique have confirmed the successful fabrication of $LiFePO_4$ composites. The unique crystal structure was thought as the main reason for the higher value of discharge capacity and better cycling performance exhibited by the synthesized octagonal prism shaped $LiFePO_4$ composites. The concepts of "order degree of arrangement" and "direction selectivity of Li-ions diffusion" were proposed first in this work, which may be well applied to explain the fact that many huge particles of $LiFePO_4$ can also exhibit excellent electrochemical performance. The especial synthetic method, the peculiar crystal structure and novel concepts are regarded as the main contributions of this preliminary work, which are believed to be meaningful for the development of lithium-ion batteries.

Acknowledgements

This work was financially supported by the National Natural Science Foundation of China (No. 21173066), Natural Science Foundation of Hebei Province of China (No.B2011205014). Z. Guo acknowledges the support from Nation Science Foundation (CMMI-13-14486).

References

[1] S.-i. Nishimura, G. Kobayashi, K. Ohoyama, R. Kanno, M. Yashima, A. Yamada, Experimental Visualization of Lithium Diffusion in Li_xFePO_4, Nat. Mater. 7 (2008) 707–711.
[2] A. Cao, A. Manthiram, Shape-controlled Synthesis of High Tap Density Cathode Oxides for Lithium Ion Batteries, Phys. Chem. Chem. Phys. 14 (2012) 6724–6728.
[3] L. Zhao, Y.S. Hu, H. Li, Z. Wang, L. Chen, Porous $Li_4Ti_5O_{12}$ Coated with N-Doped Carbon from Ionic Liquids for Li-ion Batteries, Adv. Mater 23 (2011) 1385–1388.
[4] H.-G. Jung, J. Hassoun, J.-B. Park, Y.-K. Sun, B. Scrosati, An Improved High-performance Lithium-air Battery, Nat. Chem. 4 (2012) 579–585.
[5] X.L. Wu, L.Y. Jiang, F.F. Cao, Y.G. Guo, L.J. Wan, $LiFePO_4$ Nanoparticles Embedded in a Nanoporous Carbon Matrix: Superior Cathode Material for Electrochemical Energy-storage Devices, Adv. Mater. 21 (2009) 2710–2714.
[6] A.K. Padhi, K.S. Nanjundaswamy, J.B. Goodenough, Phospho-olivines as Positive-Electrode Materials for Rechargeable Lithium Batteries, J. Electrochem. Soc. 144 (1997) 1188–1194.
[7] S. Uchida, M. Yamagata, M. Ishikawa, Optimized Condition of High-frequency Induction Heating for $LiFePO_4$ with Ideal Crystal Structure, J. Power Sources 243 (2013) 617–621.
[8] J. Liu, T.E. Conry, X. Song, M.M. Doeff, T.J. Richardson, Nanoporous Spherical $LiFePO_4$ for High Performance Cathodes, Energy Environ. Sci. 4 (2011) 885–888.
[9] M. Xie, X. Zhang, Y. Wang, S. Deng, H. Wang, J. Liu, H. Yan, J. Laakso, E. Levänen, A Template-free Method to Prepare Porous $LiFePO_4$ *via* Supercritical Carbon Dioxide, Electrochim. Acta 94 (2013) 16–20.
[10] X. Yang, Y. Xu, H. Zhang, Y.a. Huang, Q. Jiang, C. Zhao, Enhanced High Rate and Low-temperature Performances of Mesoporous $LiFePO_4$/Ketjen Black Nanocomposite Cathode Material, Electrochim. Acta 114 (2013) 259–264.
[11] Y. Xing, Y.-B. He, B. Li, X. Chu, H. Chen, J. Ma, H. Du, F. Kang, $LiFePO_4$/C Composite with 3D Carbon Conductive Network for Rechargeable Lithium Ion Batteries, Electrochim. Acta 109 (2013) 512–518.
[12] C. Sun, S. Rajasekhara, J.B. Goodenough, F. Zhou, Monodisperse Porous $LiFePO_4$ Microspheres for a High Power Li-ion Battery Cathode, J. Am. Chem. Soc. 133 (2011) 2132–2135.
[13] R. Chen, Y. Wu, X.Y. Kong, Monodisperse Porous $LiFePO_4$/C Microspheres Derived by Microwave-assisted Hydrothermal Process Combined with Carbothermal Reduction for High Power Lithium-ion Batteries, J. Power Sources 258 (2014) 246–252.
[14] Y. Wang, Y. Wang, E. Hosono, K. Wang, H. Zhou, The Design of a LiFePO4/Carbon Nanocomposite With a Core–Shell Structure and Its Synthesis by an In-situ Polymerization Restriction Method, Angew. Chem. Int. Ed. 47 (2008) 7461–7465.
[15] S. Lim, C.S. Yoon, J. Cho, Synthesis of Nanowire and Hollow $LiFePO_4$Cathodes for High-performance Lithium Batteries, Chem. Mater. 20 (2008) 4560–4564.
[16] T. Muraliganth, A.V. Murugan, A. Manthiram, Nanoscale Networking of $LiFePO_4$ Nanorods Synthesized by a Microwave-solvothermal Route with Carbon Nanotubes for Lithium Ion Batteries, J. Mater. Chem. 18 (2008) 5661–5668.
[17] Y. Zhou, J. Wang, Y. Hu, R. O'Hayre, Z. Shao, A Porous $LiFePO_4$ and Carbon Nanotube Composite, Chem. Commun. 46 (2010) 7151–7153.
[18] O. Toprakci, H.A. Toprakci, L. Ji, G. Xu, Z. Lin, X. Zhang, Carbon Nanotube-Loaded Electrospun LiFePO4/Carbon Composite Nanofibers as Stable and Binder-Free Cathodes for Rechargeable Lithium-Ion Batteries, ACS Appl. Mater. Interfaces 4 (2012) 1273–1280.
[19] A.A. Salah, P. Jozwiak, J. Garbarczyk, K. Benkhouja, K. Zaghib, F. Gendron, C. Julien, Local Structure and Redox Eenergies of Lithium Phosphates with Olivine- and Nasicon-like Structures, J. Power Sources 140 (2005) 370–375.
[20] Z. Wang, S. Su, C. Yu, Y. Chen, D. Xia, Synthesises, Characterizations and Electrochemical Properties of Spherical-like $LiFePO_4$by Hydrothermal Method, J. Power Sources 184 (2008) 633–636.
[21] K. Ding, W. Li, Q. Wang, S. Wei, Z. Guo, Modified Solid-State Reaction Synthesized Cathode Lithium Iron Phosphate ($LiFePO_4$) from Different Phosphate Sources, J. Nanosci. Nanotechnol. 12 (2012) 3812–3820.
[22] B. Wang, Y. Qiu, L. Yang, Structural and Electrochemical Characterization of $LiFePO_4$Synthesized by an HEDP-based Soft-chemistry Route, Electrochem. Commun. 8 (2006) 1801–1805.
[23] K. Ding, M. Cao, Pyrolysis of Chloroplatinic Acid to Directly Immobilize Platinum Nanoparticles onto Multi-walled Carbon Nanotubes, Russ, J. Electrochem. 44 (2008) 977–980.
[24] K. Bazzi, B.P. Mandal, M. Nazri, V.M. Naik, V.K. Garg, A.C. Oliveira, P.P. Vaishnava, G.A. Nazri, R. Naik, Effect of surfactants on the electrochemical behavior of LiFePO4 cathode material for lithium ion batteries, J. Power Sources 265 (2014) 67–74.
[25] D. Zhao, Y.-l. Feng, Y.-g. Wang, Y.-y. Xia, Electrochemical Performance Comparison of $LiFePO_4$Supported by Various Carbon Materials, Electrochim. Acta 88 (2013) 632–638.
[26] D. Ziolkowska, K.P. Korona, B. Hamankiewicz, S.-H. Wu, M.-S. Chen, J.B. Jasinski, M. Kaminska, A. Czerwinski, The Role of SnO_2 Surface Coating on the Electrochemical Performance of $LiFePO_4$Cathode Materials, Electrochim. Acta 108 (2013) 532–539.
[29] M. Chen, C. Du, B. Song, K. Xiong, G. Yin, P. Zuo, X. Cheng, High-performance $LiFePO_4$ Cathode Material from $FePO_4$ Microspheres with Carbon Nanotube Networks Embedded for Lithium Ion Batteries, J. Power Sources 223 (2013) 100–106.
[30] Y. Ding, Y. Jiang, F. Xu, J. Yin, H. Ren, Q. Zhuo, Z. Long, P. Zhang, Preparation of Nano-structured $LiFePO_4$/graphene Composites by Co-precipitation Method, Electrochem. Commun. 12 (2010) 10–13.
[31] C.M. Doherty, R.A. Carusoab, C.J. Drummond, High Performance $LiFePO_4$Electrode Materials: Influence of Colloidal ParticleMorphology and Porosity on Lithium-ion Battery Power Capability, Energy Environ. Sci. 3 (2010) 813–823.
[32] J. Ni, M. Morishita, Y. Kawabe, M. Watada, N. Takeichi, T. Sakai, Hydrothermal Preparation of $LiFePO_4$Nanocrystals Mediated by Organic Acid, J. Power Sources 195 (2010) 2877–2882.
[33] A.J. Bard, L.R. Faulkner, Electrochemical Methods, second ed., Wiley, 2001, pp. 231.
[34] B. Jin, E.M. Jin, K.-H. Park, H.-B. Gu, Electrochemical Properties of $LiFePO_4$-Multiwalled Carbon Nanotubes Composite Cathode Materials for Lithium Polymer Battery, Electrochem. Commun. 10 (2008) 1537–1540.
[35] M. Gaberscek, R. Dominko, J. Jamnik, Is small Particle Size More Important than Carbon Coating? An Example Study on $LiFePO_4$Cathodes, Electrochem. Commun. 9 (2007) 2778–2783.
[36] Z.-R. Chang, H.-J. Lv, H.-W. Tang, H.-J. Li, X.-Z. Yuan, H. Wang, Synthesis and Characterization of High-density $LiFePO_4$/C Composites as Cathode Materials for Lithium-ion Batteries, Electrochim. Acta 54 (2009) 4595–4599.
[37] K. Ding, Y. Wang, L. Liu, L. Liu, X. Zhang, Z. Guo, Hydrothermal Process Synthesized ElectrocatalyticMulti-walled Carbon Nanotubes-inserted Gold Composite Microparticles toward Ethanol Oxidation Reaction, J. Appl. Electrochem. 43 (2013) 567–574.
[38] K. Ding, K. Ding, Z. Jia, Q. Wang, X. He, N. Tian, R. Tong, X. Wang, Electrochemical Behavior of the Self-assembled Membrane Formed by Calmodulin (CaM) on a Au Substrate, J. Electroanal. Chem. 513 (2001) 67–71.